




Article

# Comparison of Intelligence Control Systems for Voltage Controlling on Small Scale Compressed Air Energy Storage

Widjonarko <sup>1,\*</sup>, Rudy Soenoko <sup>2</sup>, Slamet Wahyudi <sup>2</sup> and Eko Siswanto <sup>2</sup>

<sup>1</sup> Energy Conversion, Electrical Engineering Departement, Universitas Jember, Jalan Kalimantan No. 37, Jember, East Java 68121, Indonesia

<sup>2</sup> Energy Conversion, Mechanical Engineering Departement, Universitas Brawijaya, Jalan M.T. Haryono No. 167, Malang, East Java 65145, Indonesia; rudysoen@ub.ac.id (R.S.); slamet\_w72@ub.ac.id (S.W.); eko\_s112@ub.ac.id (E.S.)

\* Correspondence: widjonarko.teknik@unej.ac.id; Tel.: +62-813-5822-3843

Received: 3 January 2019; Accepted: 18 February 2019; Published: 28 February 2019



**Abstract:** This study presents the strategy of controlling the air discharge in the prototype of small scale compressed air energy storage (SS-CAES) to produce a constant voltage according to the user set point. The purpose of this study is to simplify the control of the SS-CAES, so that it can be integrated with a grid based on a constant voltage reference. The control strategy in this study is carried out by controlling the opening of the air valve combined with a servo motor using three intelligence control systems (fuzzy logic, artificial neural network (ANN), and adaptive neuro-fuzzy inference system (ANFIS)). The testing scenario of this system will be carried out using two scenes, including changing the voltage set point and by switching the load. The results that were obtained indicate that ANN has the best results, with an average settling time of 2.05S in the first test scenario and 6.65S in the second test scenario.

**Keywords:** ANFIS; artificial neural network; fuzzy; small scale compressed air energy storage (SS-CAES); voltage controlling

## 1. Introduction

The development of a combination of renewable energy technologies and energy storage is the most rapidly developing research topic at this time [1,2]. Problems related to the use of non-renewable energy which is still high [3] and becomes the world's main problem (especially in climate change [4]) can be solved [5,6] by using a combination of this technologies. In some applications for renewable energy use, this energy source is not used as the main support for an area's load [7,8]. However, this energy source is more widely used as a support for overcoming peak loads at certain times [7,9–15]. The reason is that, in some renewable energy sources, it is still very dependent on weather conditions, such as the use of photovoltaics (PV) [16–19], which will only produce energy during the day. Given this problem, the existence of storage technology that will store energy when the energy not in use, such as batteries, is vital [20]. However, batteries still have problems with environmental aspects because of toxic waste [21,22] and they can explode due to excessive heat [23]. Therefore, some researchers have begun to shift a lot on the topic of developing energy storage technology that is more environmentally friendly, has no degradation over time, such as batteries, and is relatively inexpensive on an energy base [1]. One of the technologies chosen is Compressed Air Energy Storage (CAES), or on a small scale known as SS (Small Scale)-CAES [3,9,24]. This technology is considered to be capable of overcoming environmental problems, because the energy source used is atmosphere gas [9,25–28], and it does not require large space, as on a large scale (CAES) [29].

To be able to help the grid in maintaining supply at peak loads, the combination of renewable energy technology and energy storage must be synchronized [30] with the network, so that energy can be transferred and not cause the grid to be damaged [31]. One of them is by controlling several parameters that are contained in the system the formed, such as frequency or voltage [32–34]. Information regarding several studies focus on controlling parameters in the SS-CAES, and can be found in the paper that has been published [35], one of which was carried out by Martinez [36,37]. In the Martinez study, he simulated the control of air valves in the SS-CAES to supply power according to the grid requirements. The simulation of SS-CAES formed was using an AC-PMSG generator (Permanent magnet synchronous generator). In that study, the generator is connected to several converters before being connected to the grid (including AC-DC converters and inverters). The control carried out is to control the pneumatic valve that is operated in the open-close mode to get the appropriate pressure in achieving the desired power. In another study that was conducted by Maia [38], the SS-CAES prototypes were made using a three-phase generator. The prototype made is observed without controlling the parameters that were contained in the SS-CAES. In another study that was conducted by Kokaew, V. [39–41], it controlled the rotational speed rotation parameters in the SS-CAES prototype. Fighting the mechanical torque that arises because the air passing through the airmotor with electric torque is regulated using a Buck converter carries out speed regulation. The purpose of this control is to get the speed referenced in achieving maximum power transfer or known as MPPT (Maximum power point tracking). However, from several previous studies, no research discusses how SS-CAES can produce a constant voltage to be indirectly integrated into the grid [5,12]. Whereas, in some concepts that have been put forward by several researchers, such as Vongmanee [42], Lemofouet [43], and Martinez [37], to be able to integrate the SS-CAES system into the grid, it must be combined with an inverter. In the general concept, the inverter requires a specific DC input voltage to operate by the voltage parameters on the grid. Therefore, to facilitate integrated systems, energy sources must adjust the inverter's working voltage or it has a stable voltage [44–46], and the energy can be transferred to the grid.

However, in detailed research, Martinez has published his research [36,37] to integrate his system. The strategy that was used by Martinez in his simulation is to control the air pressure using pneumatic valves to reach the required power. However, in the results of his study, the power had a high and low effect because of the pneumatic open-close mechanism. This results happened, because the air pressure that entered the turbine (air motor) is controlled by an open-close mechanism, so that the power also has the same characteristics [36,37]. Because of this phenomenon, the inverter will have to done two jobs. The first is to stabilize the voltage and the second is to synchronize with the phase on the grid. These multiple actions cause the control system that is used to be more complicated.

To be able to simplify the control and eliminate the effects that are caused by the previous study, the changes will be made in this study. There are two strategies used in this study to solve that problem. The first is to remove the high-low effect in previous studies, that is replacing the pneumatic valve control with a combination of valve and servo motor. By using this way, the airflow rate will have smoother air transfer and will also make the produced voltage smoother, so the high-low effects can be eliminated. This could be happened because the control concept using a servo motor works by adjusting the direction of the rotation rather than an open-close mechanism such as in pneumatics system. The second is to replace the control reference to a voltage reference. Thus, the integration between SS-CAES and the grid will be much easier, since the inverter will only adjust the network phase rather than doing two actions (voltage and phase synchronization according to the previous research). Since the controlled system has a high workload, the system is very susceptible to parameter changes and input disturbances. Those issues will be a big problem if a conventional model is used to control the system, therefore artificial intelligence (AI) is chosen. By using AI, the system will be able to work with robust controls and can adapt to non-linear systems [47]. Some AI systems that will be used in the system must have these criteria, there are Fuzzy Logic, Artificial Neural Network, and adaptive neuro-fuzzy inference system (ANFIS). In this study, an experiment will be done to compare the use of

these three AIs to control the SS-CAES prototype with 60W that has been built by the researcher to reach the desired set point voltage of the user. The purpose of comparing the performance of the three AIs is to be able to find out the most appropriate control system to solve this problem. In this study, the system has been tested with two scenarios for testing the settling time variable by implementing a microcontroller that was programmed with three artificial intelligence, as a control device.

## 2. Small Scale Compressed Air Energy Storage Design

### 2.1. Prototype Design

The SS-CAES system prototype block diagram that can be schematically seen in Figures 1 and 2 is a picture of a prototype made. Several SS-CAES components, including air tanks, air valves (which combine with continuous servo motors), air motors, and DC generators form the system [38] (Figure 2a). In this study, several sensors were installed to retrieve the response from the control system. Some of these parameters are voltage, current, air pressure passing through air-motor, and speed sensor. Data associated with these parameters will be saved in the data logger to observe the effect of changes in the control process that was carried out.

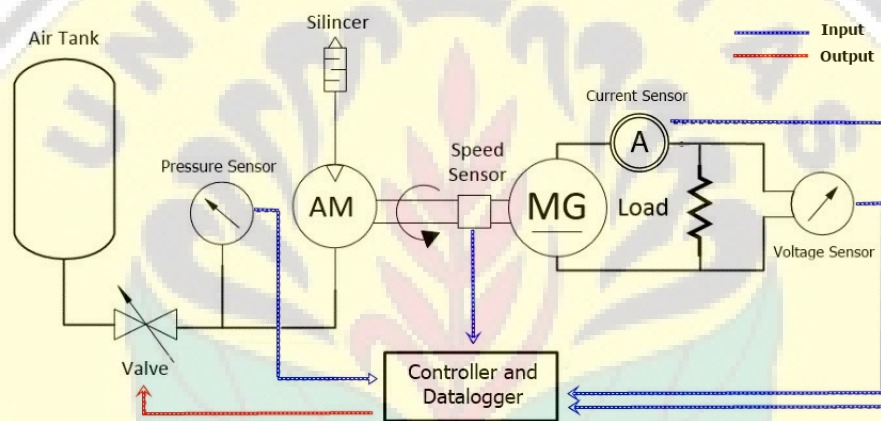
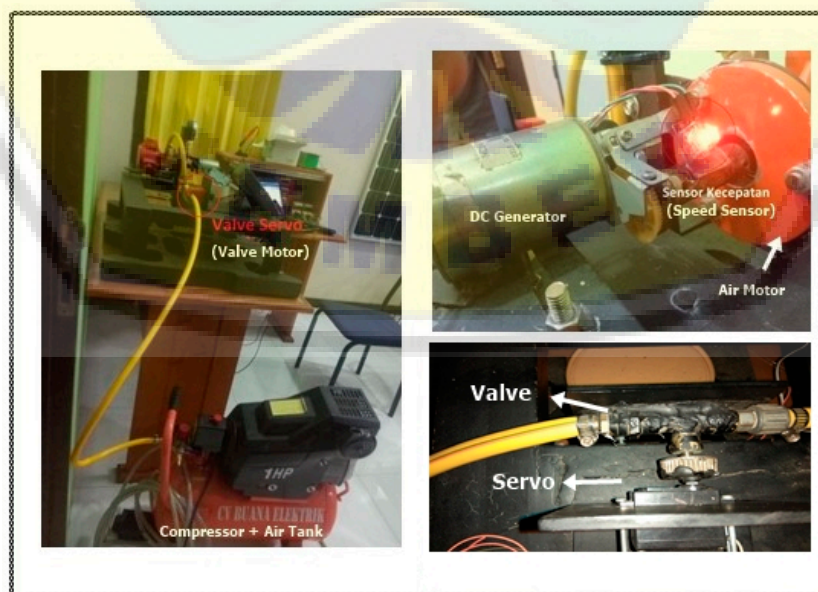
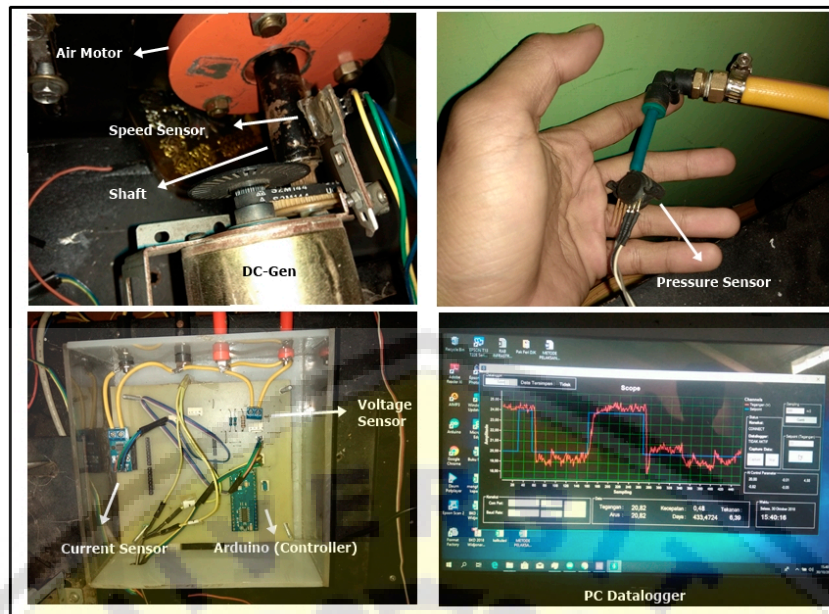


Figure 1. Block diagram of prototype small scale compressed air energy storage (SS-CAES).



(a)

Figure 2. Cont.



(b)

**Figure 2.** (a) The main components of prototype SS-CAES; and, (b) The installed sensor, controller on prototype SS-CAES and PC data logger.

In this study, there are four types of sensors that are used in the prototype. The first one is the voltage sensor that is made using the principle of the voltage divider; the second is the speed sensor that uses a hall effect sensor. The third is the air pressure sensor using MPX 5010 (Freescale Semiconductor, Inc., Austin, TX, USA), and the fourth is the current sensor using ACS712. All of the sensors used in this test have been calibrated so the value that appears on the sensor is the real value of the measured parameter. This experiment was done using a servo that was controlled and coupled with an air valve; the servo type that was used in this experiment is MG 996R (TowerPro, Singapore City, Singapore). For the controller, the Arduino UNO microcontroller is used, which is connected to the Computer (monitoring, controlling, and data logger function). Since the primary target of this study is to stabilize the voltage to connect an inverter, then the load used is a resistor with a value of  $150 \Omega$ . Figures from sensors, controllers, and PC data loggers can be seen in Figure 2b. Details of the control mechanism of this prototype will be explained in the control block section.

## 2.2. Control Block

There are four sensors installed on the prototype, but only one sensor will be used as a control reference, which is the voltage sensor. Even so, all the data from the sensor will be saved in the data logger. These data were used to analyze the system performance. The reason for using one sensor in this study is because this system implemented a closed-loop control system where one of the inputs is used in the controlling system as a feedback control from the plant [48]. A detailed scheme of this control block can be seen in Figure 3.

Figure 3 shows that there are two parameters that are used as inputs in this control system. The first parameter is the set point voltage, as determined by the user, and the second parameter is the output voltage (from voltage sensor) of the prototype. To fulfill the closed-loop control system, the input is changed to become two control inputs from the system. These two inputs are Error and Delta Error [48,49], where we can use Equations (1) and (2). After the Error and Delta Error value are obtained, the value of the two parameters will be processed in the controller block. The controller that was used in this prototype was the Arduino UNO microcontroller, as described earlier. This microcontroller will be programmed with three different artificial intelligence according to the scenario

that will be tested at the plant. The output of this controller is a pulse width modulator (PWM) signal. The PWM signal is used to control the air valve combined with a servo motor.

$$e(t) = \text{Set Point} - \text{Actual Voltage} \tag{1}$$

$$de = e(t) - e(t - 1) \tag{2}$$

where  $e$  is Error,  $de$  is DeltaError,  $e(t)$  is Error at time  $t$ , and  $e(t - 1)$  Error in time  $t - 1$  or time before.

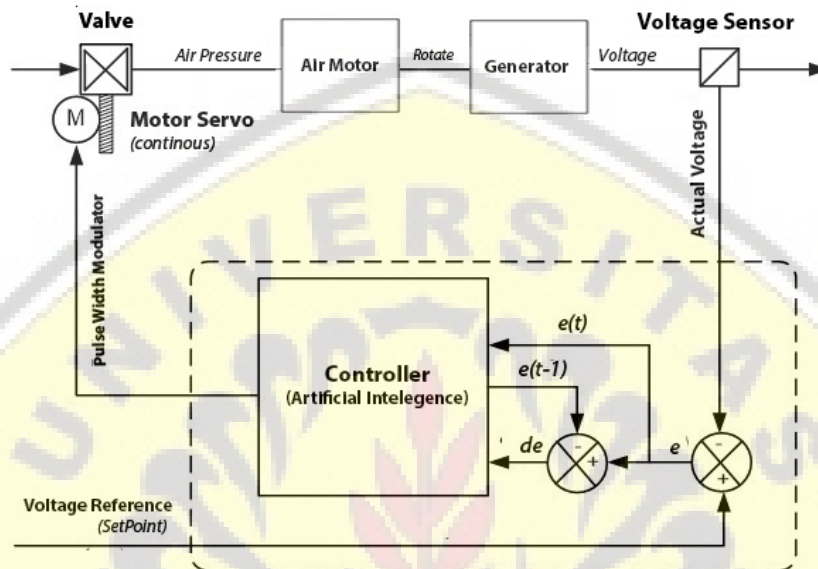


Figure 3. Control block of prototype SS-CAES.

To achieve a constant voltage, the key is to control the airflow entering the system. This condition can be achieved because of the characteristics of the SS-CAES where the voltage generated is directly proportional to the speed of the air motor [40,50]. The faster that the generator changes its speed, the higher the voltage will be generated. Because the rotation speed of an air motor needs to be controlled, it is done by controlling the rate of airflow through the air motor. Therefore, the key to control the voltage is to adjust the airspeed by controlling the valve.

The valve that was used in the prototype is a combination of air valves and a continuous servo. The width of the airline on the valve can be adjusted to control the rate of the airflow, this can be done by changing the servo rotation. However, in continuous servo control, it differs slightly from the general servo. In the continuous servo, the rotation control is not based on the desired angle but rather is based on the direction of rotation (rotating clockwise or counterclockwise). From the servo that was installed in this study, to widen the valve opening, the servo must be controlled clockwise by giving a PWM value  $>100$ . Whereas to reduce valve openings, the servo must be controlled so that it rotates counterclockwise, that is by providing a PWM value  $<100$ . To stop the rotating servo, PWM = 100 is given. It should also be noted that, the higher the PWM value of the neutral value when the servo stops (PWM = 100), the faster the servo rotation goes in that direction. For example, when PWM = 105, the servo will move quickly in a clockwise direction with different speeds with PWM = 101, and so does the opposite direction. As for the AI, the control output value is the number of actual PWM values with PWM AI output control. For more details, see Equation (3).

$$\text{PWM}(t) = \text{PWM}(t - 1) + \text{PWM}(\text{AIOutput}) \tag{3}$$

where the  $\text{PWM}(t)$  is the actual output of the PWM,  $\text{PWM}(t - 1)$  is PWM value in time  $t - 1$  or time before, and  $\text{PWM}(\text{AIOutput})$  is the PWM of the AI process.

### 3. Intelligence Controller

There are three artificial intelligence systems that are used in this study. The explanation and design of the artificial intelligence system are explained in this subsection.

#### 3.1. Fuzzy Logic Controller

Fuzzy Logic is a rule-based decision-making process that aims to solve problems, where systems are difficult to model or where there is ambiguity [51,52]. Fuzzy logic is determined by logical equations, not from complex differential equations and it comes from thinking that identifies and utilizes obscurity between two extreme lines. Fuzzy logic systems consist of fuzzification, defuzzification, rule base, and inference systems [47]. Fuzzy can work according to the rules that are given by fuzzy designers. By using rules, the relationship between the input that enters the system can be known for its output value. The structure of processing fuzzy logic can be seen in Figure 4.

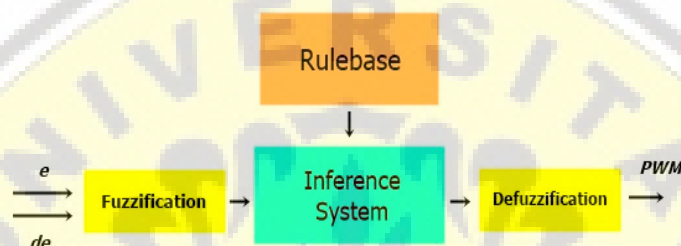


Figure 4. Structure of fuzzy logic controller.

In designing the control system using Fuzzy Logic, the number of membership input and output members is 5, including NB (Negative Big), NS (Negative Small), Zero, PS (Positive Small), and PB (Positive Big). For each membership value, the value of the input (Error and Delta Error) can be seen in Figures 5 and 6. While, for membership, output can be seen in Figure 7.

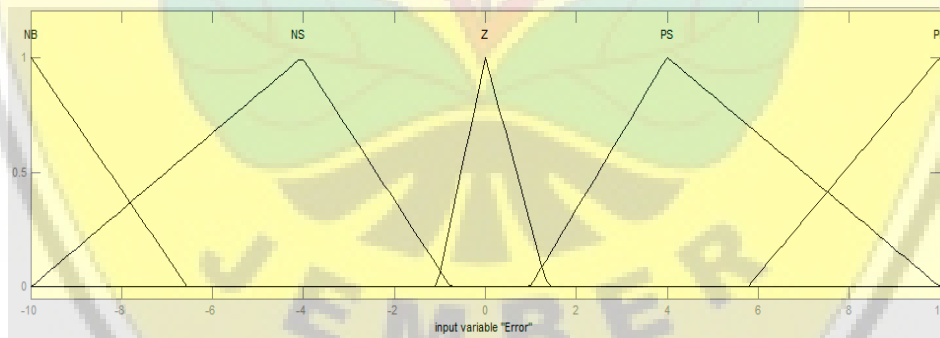


Figure 5. Membership input of error.

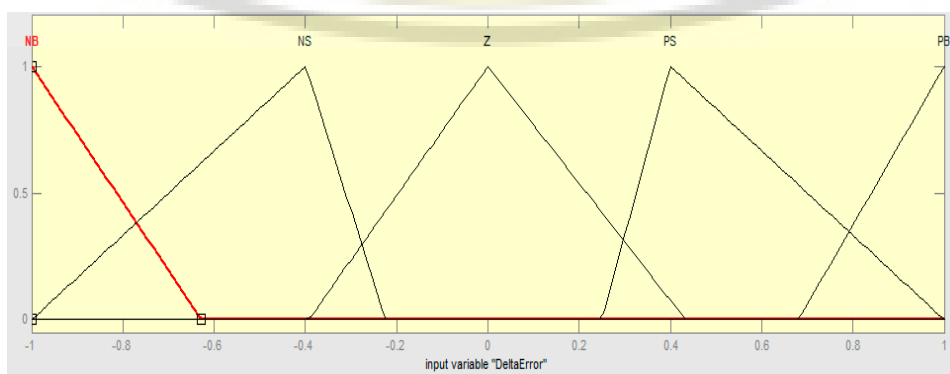


Figure 6. Membership input of delta error.

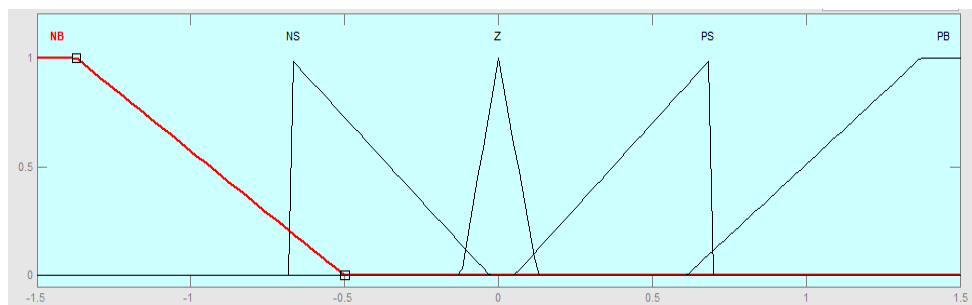


Figure 7. Membership output of pulse width modulator (PWM).

### 3.2. Artificial Neural Network

Artificial neural network (ANN) is an information processing technique or approach that is inspired by the workings of the biological nervous system, especially in the cells of the human brain in processing information [53,54]. A key element of this technique is the unique and diverse structure of information processing systems for each application. The Neural Network consists of a large number of information processing elements (neurons) that are interconnected and work together to solve certain problems [55]. In this study, the Artificial Neural Network (ANN) was used with the architecture, as shown in Figure 8.

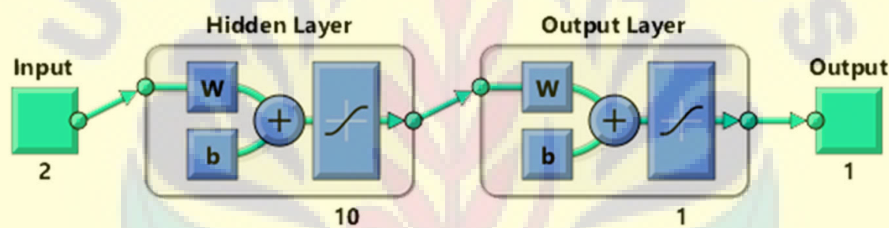


Figure 8. Architecture of artificial neural network used in this study.

The ANN structure that was built by researchers consists of two inputs, namely error and delta error. For the layer used, there are two layers with ten neurons for the hidden layer and one neuron for the output layer with output that is in the value of PWM. The activation function that is used in this structure uses sigmoid activation. The structure of the hidden layer can be seen in Figure 9, while for the whole structure, it can be seen in Figure 10.

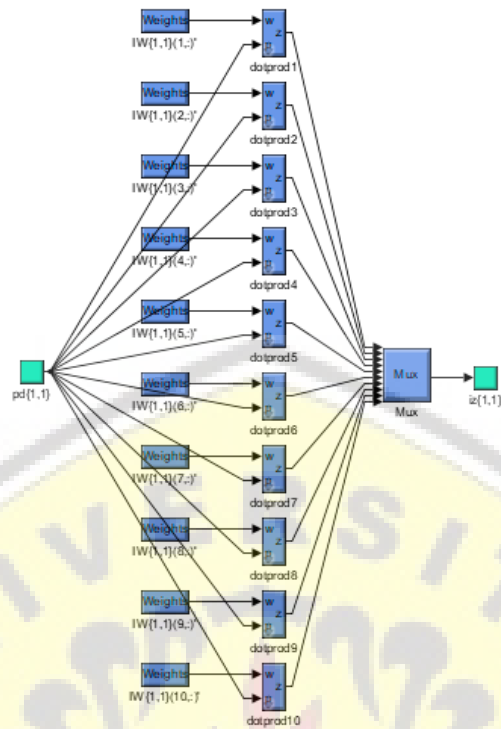


Figure 9. Structure of hidden layer artificial neural network used in this study.

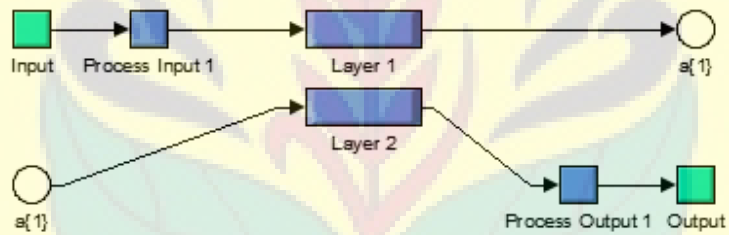


Figure 10. Structure of artificial neural network used in this study.

Artificial neural networks are built using the Levenberg–Marquardt back propagation training algorithm. The training data to create a network is obtained from conventional control data that was applied to the plant. The total data used is  $3 \times 816,160$  with a portion of training data for 70%, while 15% of the data is for testing and validation. The relationship between training, testing, and network validation formed by ANN has a high correlation coefficient and it can be seen in Figure 11.



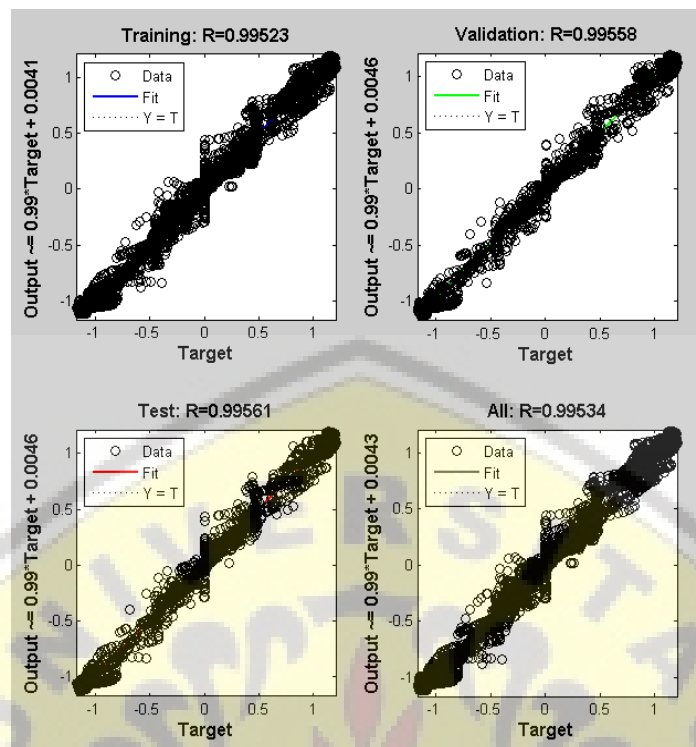


Figure 11. Regression plot of Artificial Neural Network (ANN).

### 3.3. Adaptive Neuro Fuzzy Inference System

The adaptive neuro-fuzzy inference system (ANFIS) is a method that uses artificial neural networks to implement fuzzy inference systems. The advantage of the fuzzy inference system is that it can translate knowledge from experts in the form of rules, but it usually takes a long time to determine membership functions [47,56]. Therefore, learning techniques from ANN are needed to automate the process, so that it can reduce search time; this causes the ANFIS method to be very well applied in various fields [57].

The ANFIS structure that was used in this study uses two inputs, namely error and delta error. While, from the results of the ANFIS training, nine rules will be applied for the implementation of the prototype. The ANFIS structure in this study can be seen in Figure 12.

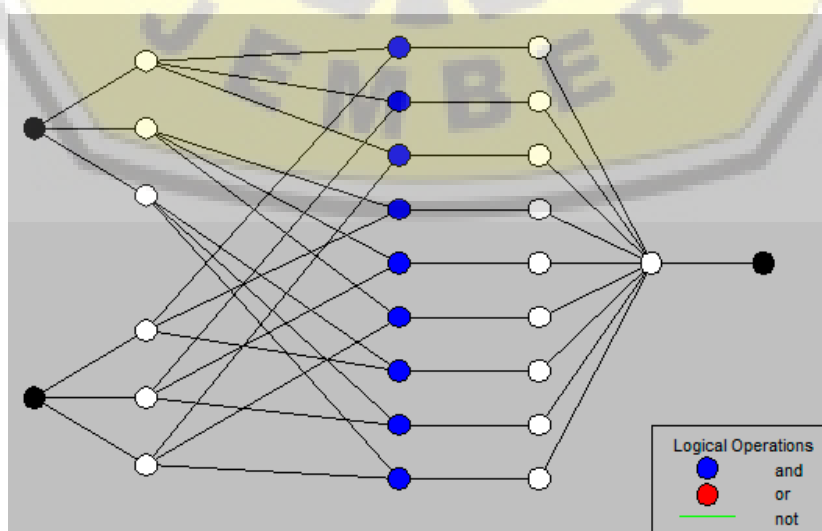


Figure 12. Structure of adaptive neuro-fuzzy inference system (ANFIS).

#### 4. Testing Scenario

This system will be tested in two scenarios with a different AI control program on each test. The first test is to change the set point value. The experiment flowchart for the first scenario can be seen in Figure 13. In this first scenario, the system will be programmed with one of the AI controllers. Subsequently, the prototype will run with the initial set point value of 24 V. After the initial set point is reached, the set point will then be adjusted to 20 V. As long as the system reaches the steady state, all of the installed sensors data, set point values, and system response values (PWM Value) will be saved in the data logger. The purpose of saving these data is to see and analyze the response of data in offline mode (after the system has been tested). Afterwards, after 10 s or more, when the system has reached steady state, the set point value will be reduced. The set point that was previously set at 20 V decreased to 15 V. Subsequently, the cycle data is being saved while the system is running to reach a steady state again. After 10 s or more, after the system reached a steady state, the set point testing model changed. In this section, the set point will be set to higher value. This test starts by using the previous set point, which starts from 15 V, and then the set point is raised to 20 V. As the previous test, all installed sensor data, set point value, and system response will also be saved into the data logger. After 10 s or more, after the system has reached steady state, the set point value will be increased to 24 V. Afterwards, the data saving cycle is taken again while the system running to reach the steady state. After the system reached the steady state point, at the last stage, the system will be set to do final set point jump. The set point jump is from 24 V to 15 V. If we sort the set point test, it will be 24 V, 20 V, 15 V, 20 V, 24 V, 12 V, 24 V, and 15 V. These set point options are based on the voltage that is commonly used by the inverter in the grid application. The first AI Control test has been done for the first scenario. To be able to compare and see the overall AI control response that was used in this study, the first scenario will be repeated three times for three AI controls.

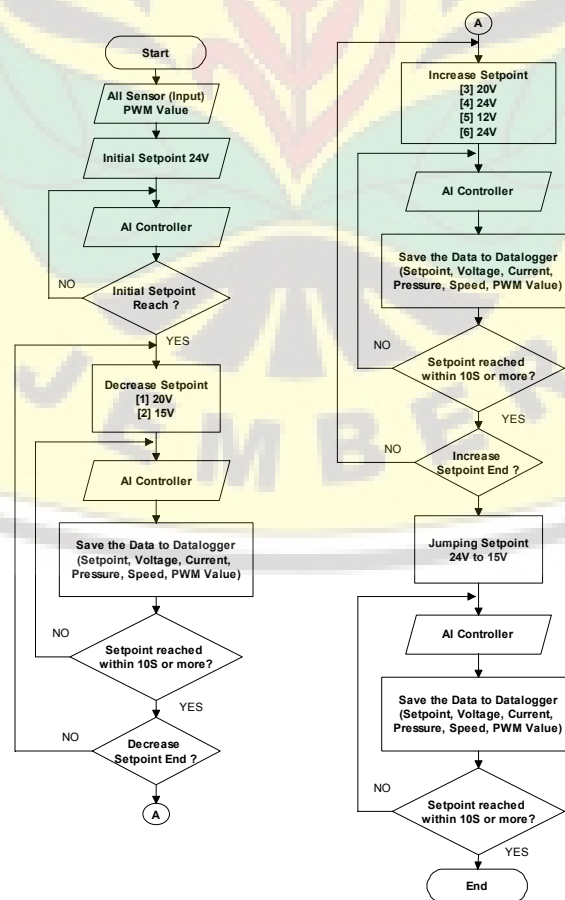


Figure 13. Flowchart Scenario 1.

For the second scenario, the system will be tested by keeping the set point given by the user. In this test, after the AI control is programmed into the microcontroller, the system will run where the system has to maintain a set point value of 20 V. At the initial condition, the 150 Ω load is not connected to the circuit. After the system reaches steady state at 20 V, then the load is connected to the circuit. Due to changes in the load, a change in voltage value occurred. During the process towards the steady state, the entire installed sensor data, voltage set point, and system response (PWM value) will be saved in the data logger. After 10 s or more, the system will reach a steady state condition, then the load will be released afterwards, and the cycle data saving process will be repeated for offline analysis. This process will be repeated three times in one experiment (switch and release load) to obtain the system response. The goal of this test is to determine the reliability of the system. That process is only testing for one cycle in the second scenario. To be able to test and see the overall AI control response that was used in this study, the first scenario will be repeated three times for three AI controls. The flowchart of the overall test in the second scenario is shown in Figure 14.

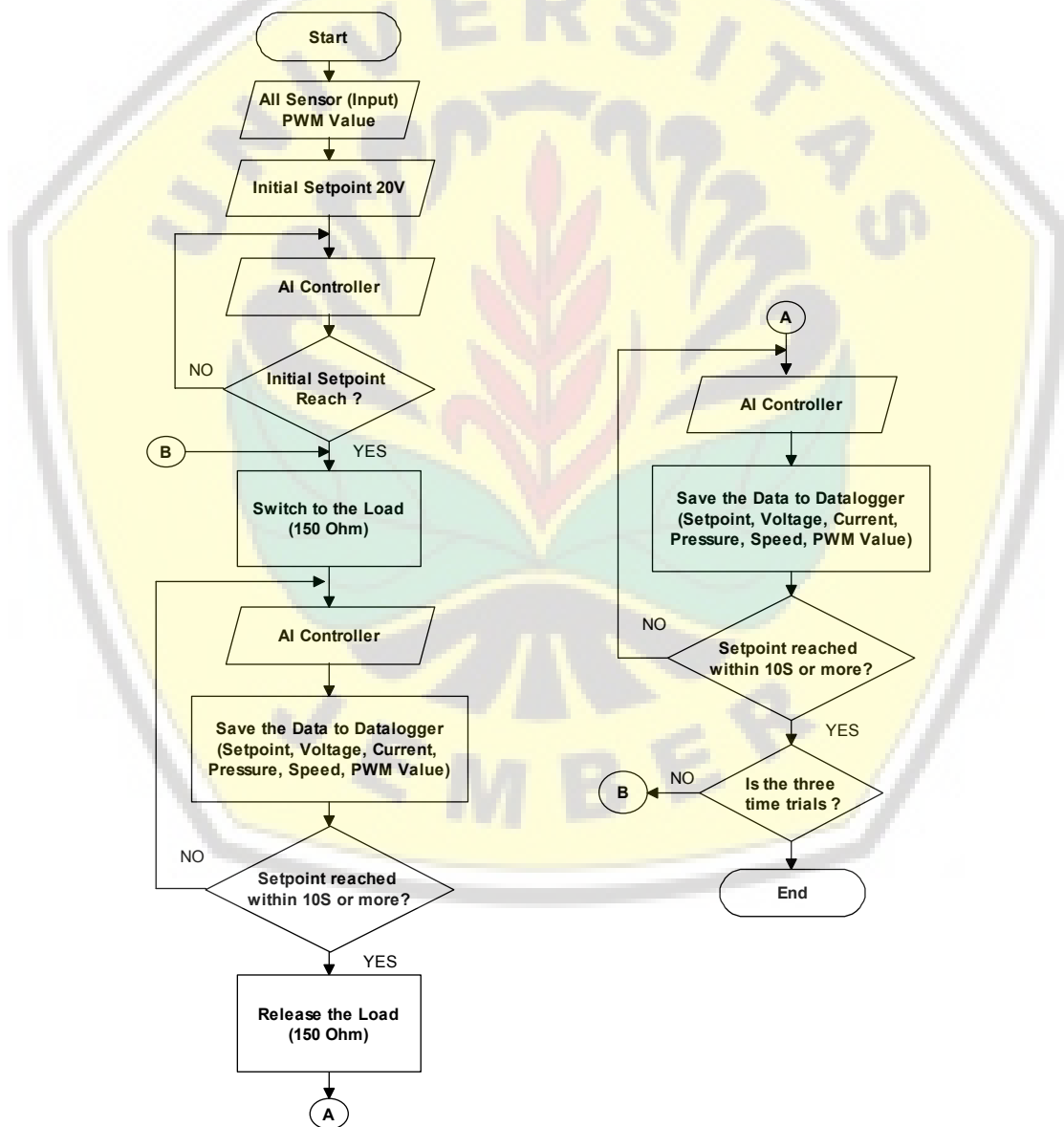


Figure 14. Flowchart Scenario 2.

## 5. Result and Discussion

In the experiment section, the SS-CAES prototype will run according to the predetermined scenario. The total number of trials is six experiments with different AI systems. The results of these experiments can be seen in Figures 15–26. The results in these figures are obtained data from the data logger that saved while the system was running according to the tested scenario.

The first test uses fuzzy logic. The system is tested with some scenarios and the obtained results can be seen in Figures 15–19. For the first scenario, the set point is changed in an order that already explained in the previous section. From the obtained data, the results shows that, to reach steady-state condition in the first scenario, fuzzy logic has an average settling time of 2.27 s. This result can be seen in Figures 15 and 16, which have been zoomed at 64 to 68 s.

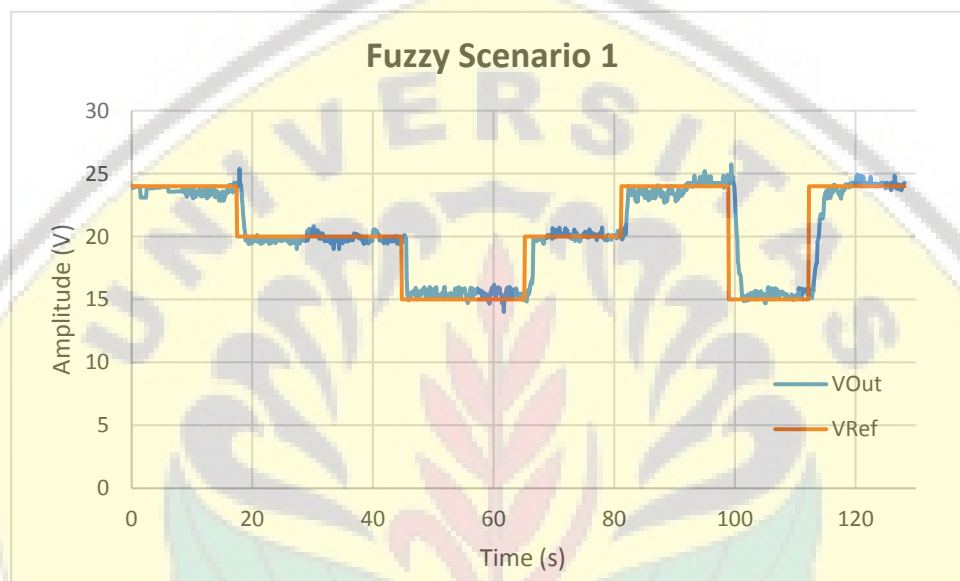


Figure 15. The results of set point changes with fuzzy logic controller.

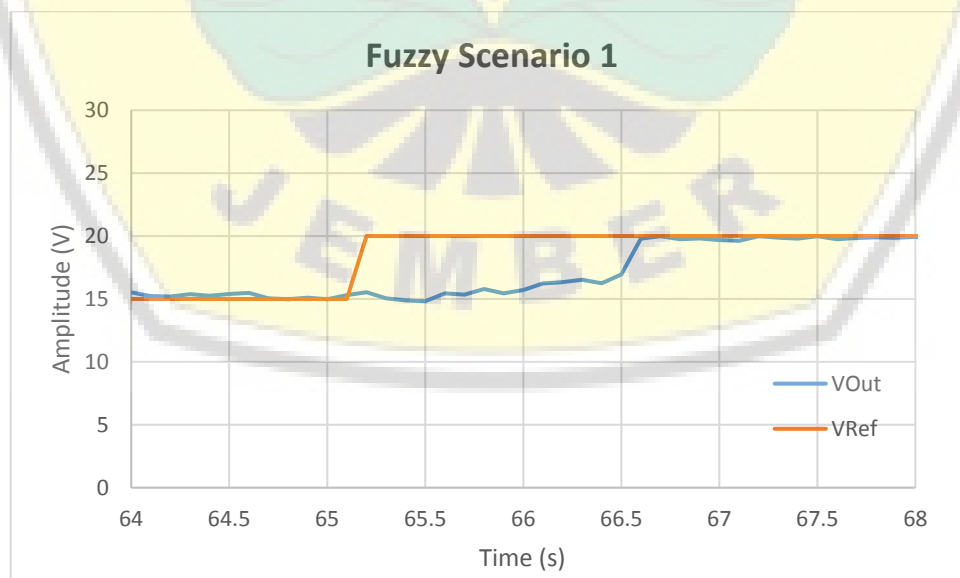


Figure 16. The results of set point changes with fuzzy logic controller on 64 to 68 s.

The results for the second test on the Fuzzy Logic Controller are shown in Figure 17. This scenario testing is done by removing the load three times and connecting the load two times. The effect that is caused by the release of the load is a surge in the output voltage with the highest value of 31.6 V. While

the impact caused when adding the load is a reduction in the output voltage with the lowest value of 14.4 V. The average settling time on the results of this test is 8.18 s. For detailed results of displacements transitions, we have presented the zoomed results on a time scale of 85–125 s in Figure 18.

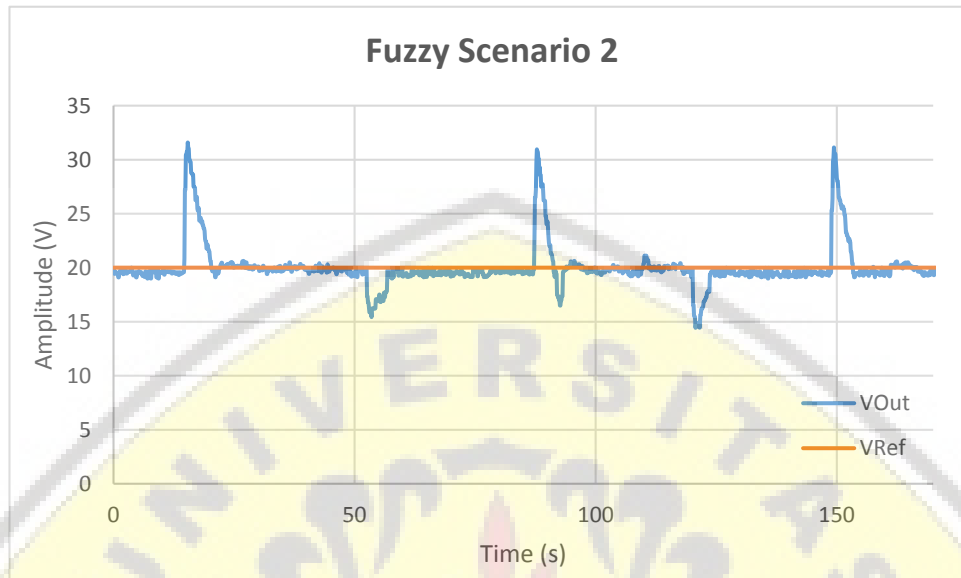


Figure 17. The response results of load changes with fuzzy logic controller.

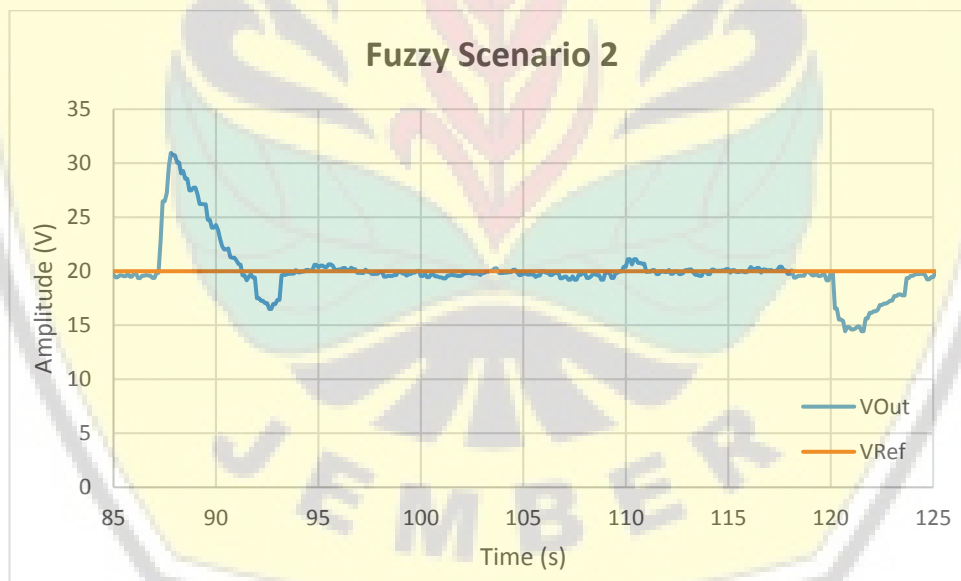


Figure 18. The results of set point changes with fuzzy logic controller on 85 to 125 s.

The next experiment is testing the artificial neural network. The first scenario can be seen in Figure 19. This scenario test resulted in an average settling time of 2.05 s. For a detailed result, we presented data that zoomed at 118–122 s in Figure 20.

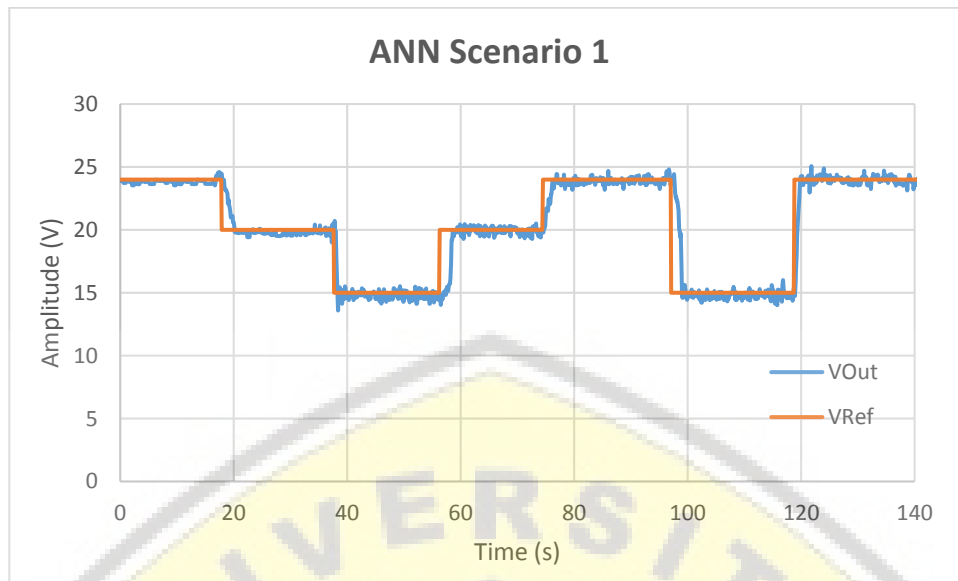


Figure 19. The response results of set point changes with artificial neural network.

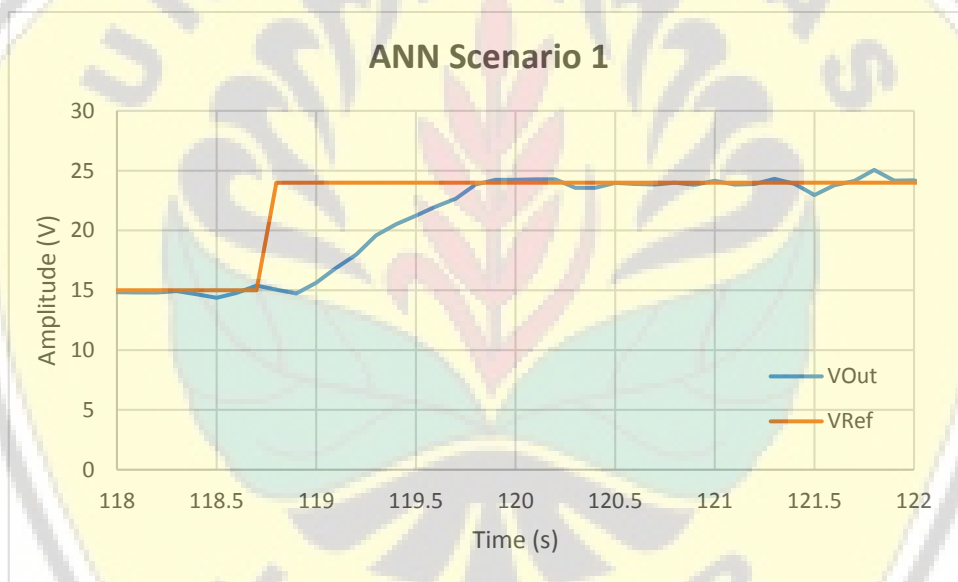


Figure 20. The response results of set point changes with artificial neural network controller on 118 to 122 s.

At the second scenario, the highest jump in the output voltage due to the load is released at 37.6 V, and the lowest voltage drop due to the load is connected at 14.7 V. The average settling time is 6.65 s. The results of this test can be seen in Figure 21. The zoomed result at 135–195 s can be seen in Figure 22.

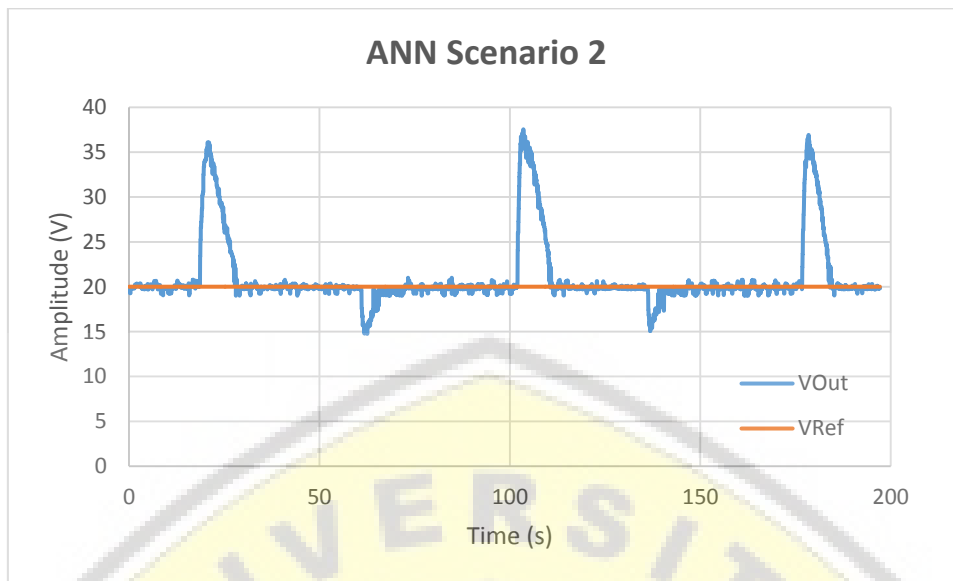


Figure 21. The response results of load changes with artificial neural network controller.

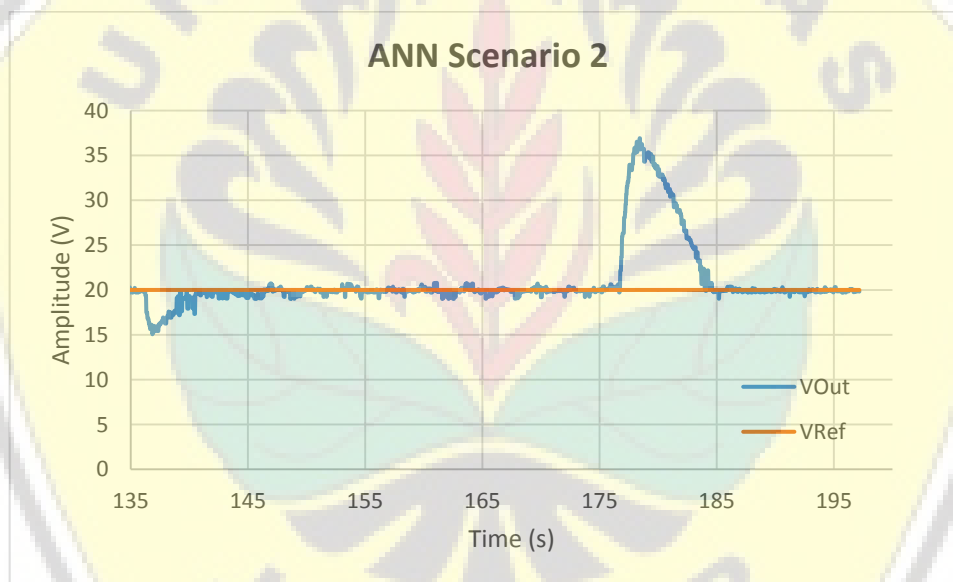


Figure 22. The response results of load changes with artificial neural network controller on 135 to 195 s.

The last experiment used ANFIS and the results can be seen in Figure 23. The first scenario test resulted in an average settling time of 3.49 s. The zoomed result at 56–60 s can be seen in Figure 24.

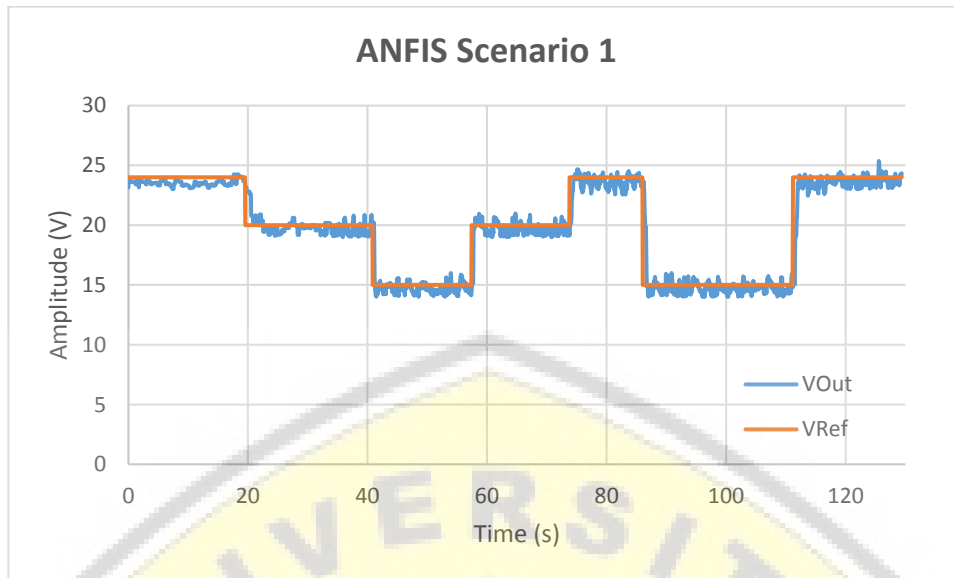


Figure 23. The response results of set point changes with ANFIS controller.

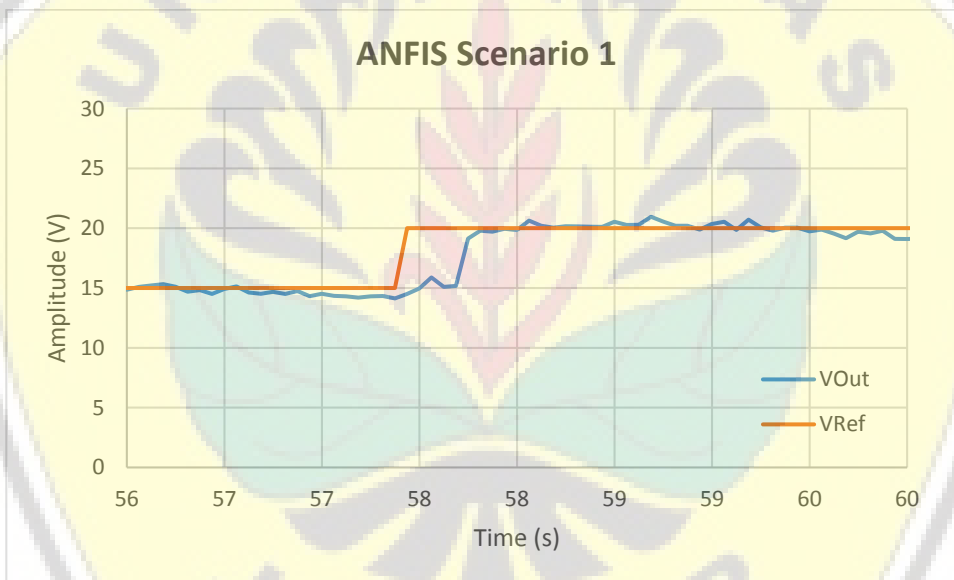


Figure 24. The response results of set point changes with ANFIS Controller on 56 s to 60 s.

For experiments using the second scenario of ANFIS, the system response can be seen in Figure 25. This test resulted in a voltage surge with the highest value of 31.6 V and the lowest voltage at 15.43 V. The average settling time in this test is 8.92 s. Figure 26 shows the results of the second scenario testing zoomed at a 145–210 s time scale.



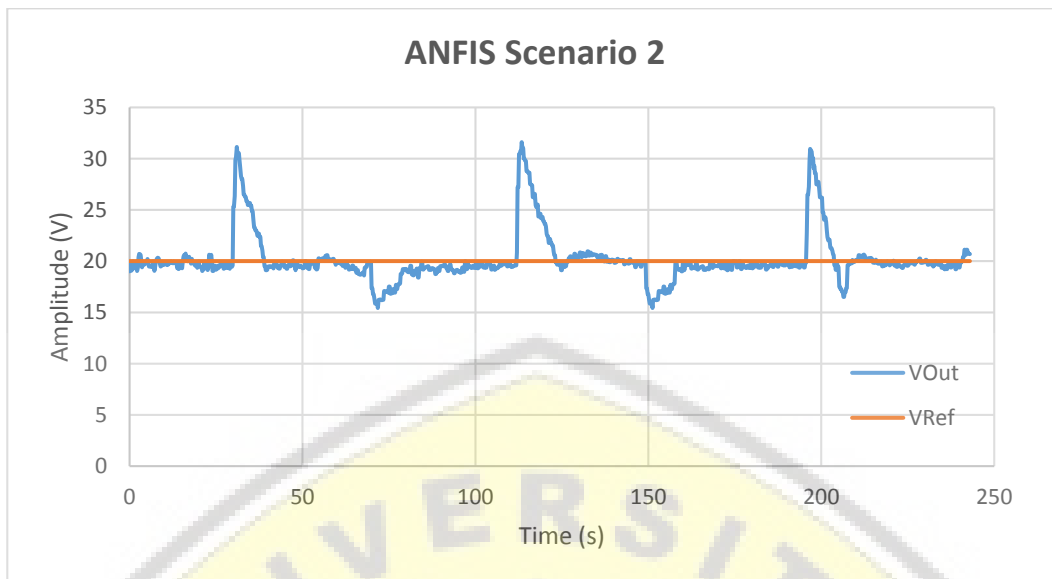


Figure 25. The response results of load changes with ANFIS controller.

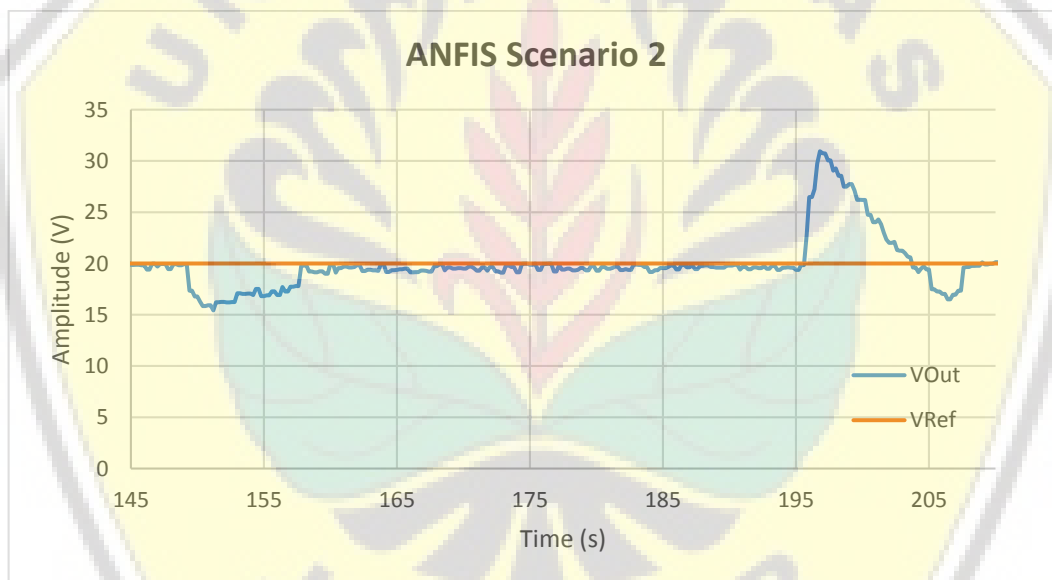


Figure 26. The response results of load changes with ANFIS Controller on 145 s to 210 s.

Those experimental results show that the best result for the first scenario (changing voltage set point) that was achieved by using ANN with an average settling time of 2.05 s. While for the second scenario (maintaining voltage), the best results were also achieved by using ANN with an average settling time of 6.65 s to reach steady state conditions. The time comparison of the results for two scenarios of the three Artificial Intelligence systems can be seen in Figure 27.

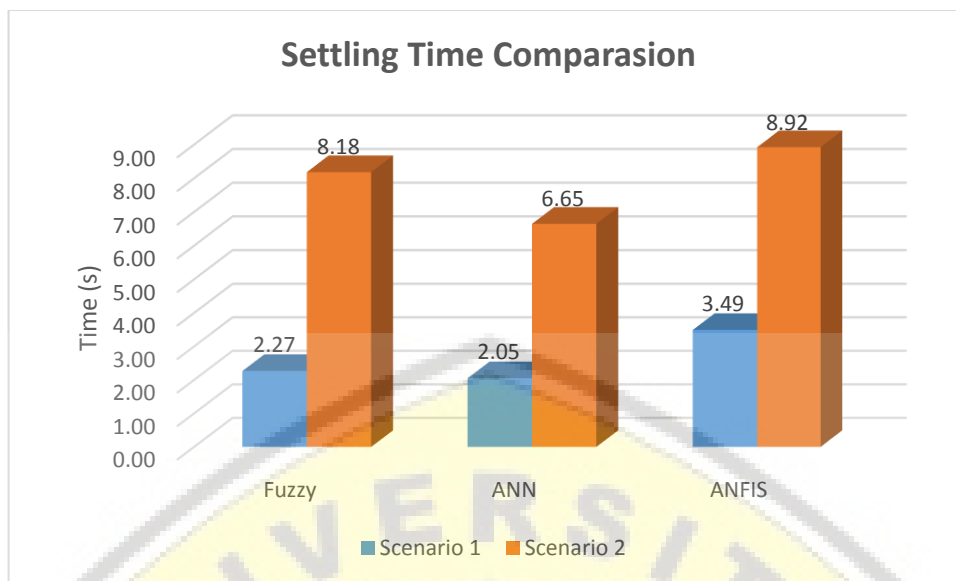


Figure 27. Settling time comparison on three intelligent control systems.

From the acquired results that are presented in Figure 27, the results show that the difference between intelligent control systems has relatively small time differences. By evaluating the first test between Fuzzy and ANN, the time difference is very close to 1 s and, when compared with ANFIS, the time difference is less than 1 s. In the second scenario, the time difference is also around 1–2 s. This difference can be occurred because of the iterative problems in each intelligent control. ANN is superior to other AI because the ANN program has shorter iterations than others, this made ANN more responsive when compared to other intelligent control systems.

If we evaluate the test results in the second scenario, we will find a high overshoot value. The high overshoot value that occurred in the second scenario was caused by the high pressure when the circuits are loaded with a 150  $\Omega$  resistor. This overshoot can be seen in Figure 25, which shows a graph of the comparison between voltage and pressure in the ANN test for the second scenario. At the early stage, the load is installed; therefore, the pressure rises to 0.36 bar. Subsequently, the load is released, the voltage does not immediately go down, but it rises for a short period before it starts to drop. This effect happened because the electrical force that opposes the mechanical force suddenly drops due to the load being released, and this caused a high shaft rotation that resulted in high generator rotation and generating high voltage. The voltage decreases corresponding to the shaft rotation that was coupled with the generator. The generator slowly decreases its speed, even though the pressure through the air-motor has been drastically reduced. As shown in Figure 28, the voltage drops slowly, which corresponds to the shaft rotation. In Figure 28, the pressure value has been multiplied by 100 to simplify the analysis process.

The graph shown in Figure 29 is about the comparison of settling time for each cycle of ANN testing Scenario 2. The number shown on each cycle is based on Figure 28. The results show that the longest cycle to normalize towards steady state is the first Cycles 1, 3, and 5 (cycles when the load is released). While Cycles 2 and 4 have a shorter settling time than others. This results shows that the problem of shaft rotation after the load is removed is one of the variables that must be resolved to accelerate the normal process.

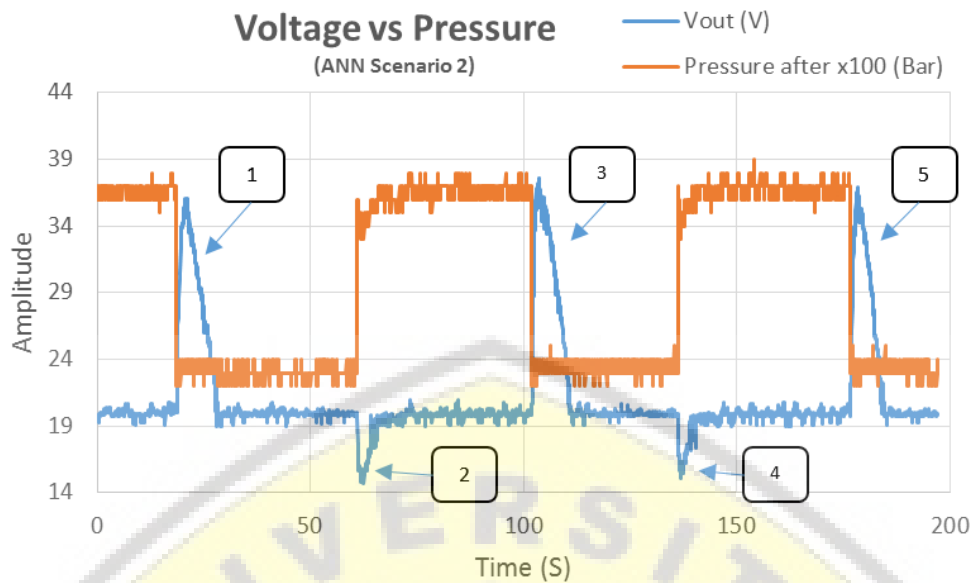


Figure 28. Comparison of voltage and pressure on the ANN scenario.

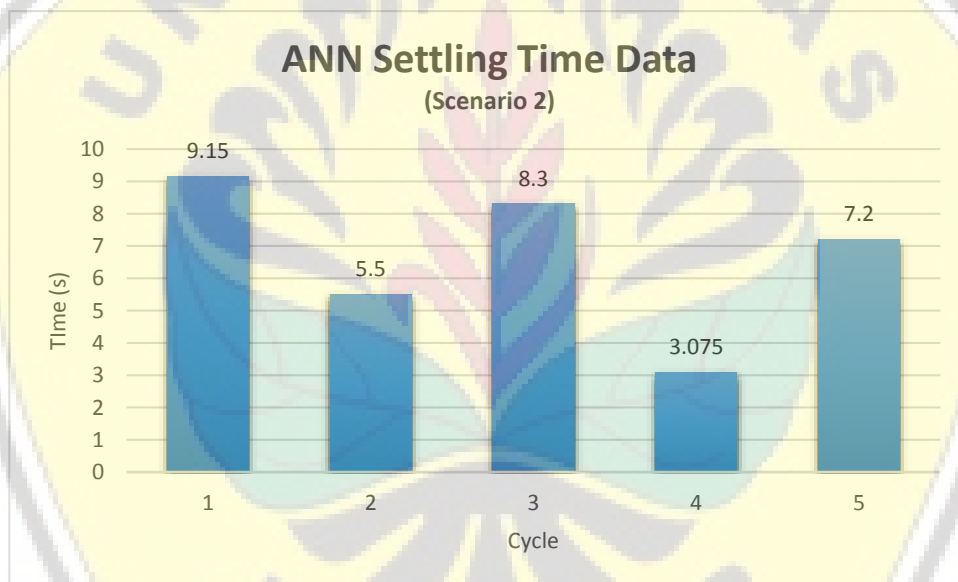


Figure 29. Comparison of settling time on each cycle in ANN scenario.

## 6. Conclusions

In this paper, an experimental evaluation is done to stabilize the voltage that is generated by the SS-CAES, so that it can be integrated into the grid indirectly. The voltage is controlled by converting air passing through the airmotor using a valve combined with a servo motor. This experiment also applied three artificial intelligences; Fuzzy Logic, ANN, and ANFIS.

This experiment uses two scenarios, the first scenario was done by changing the set point and the best results was obtained by using ANN with the average settling time of 2.05 s. The second scenario was done by connecting the load and specifying which load has the best results, as obtained using ANN 6.65 s. Those results could happen because ANN has less iteration than other intelligent controls, and this made the processing have a fast response. However, in the second scenario, there is a high overshoot value when the load was released. This overshoot is happened due to the effect of high pressure when the load was still installed. Accordingly, when the load was released, the electric torque drops suddenly and it caused the air motor to spin again tight, since the remaining mechanical energy was still high. Overall, the results shows that the system successfully stabilized the voltage smoothly.

**Author Contributions:** Widjonarko has proposed, conceptualization and written the remaining manuscript. R.S., S.W. and E.S. as validated the main idea and supervision. All authors together organized and refined the manuscript in the present form.

**Funding:** This research is supported by the LPDP scholarships under grant No. 20161141011767. The author gratefully acknowledges Universitas Brawijaya for the support for this research.

**Conflicts of Interest:** The author declares no conflict of interest.

## Nomenclature

AI	Artificial intelligence
AM	Air motor
$b$	Bias
$de(t)$	Delta error
$e(t)$	Error
$e(t - 1)$	Error in time before
MG	Motor generator
$PWM(t)$	Pulse Width Modulator (actual output)
$PWM(t - 1)$	Pulse Width Modulator (actual output in time $t - 1$ )
$PWM(AIOutput)$	Pulse Width Modulator from AI output process
$V$	Voltage, V
$V_{Out}$	Voltage output, V
$V_{Ref}$	Voltage reference, V
$w$	Weight

## References

- Alhamali, A.; Farrag, M.E.; Bevan, G.; Hepburn, D.M. Review of Energy Storage Systems in electric grid and their potential in distribution networks. In Proceedings of the 2016 Eighteenth International Middle East Power Systems Conference (MEPCON), Cairo, Egypt, 27–29 December 2016; pp. 546–551.
- Ubertini, S.; Facci, A.L.; Andreassi, L. Hybrid Hydrogen and Mechanical Distributed Energy Storage. *Energies* **2017**, *10*, 2035. [[CrossRef](#)]
- Luo, X.; Wang, J.; Dooner, M.; Clarke, J. Overview of current development in electrical energy storage technologies and the application potential in power system operation. *Appl. Energy* **2015**, *137*, 511–536. [[CrossRef](#)]
- Li, W.; Kong, D.; Wu, J. A New Hybrid Model FPA-SVM Considering Cointegration for Particular Matter Concentration Forecasting: A Case Study of Kunming and Yuxi, China. *Comput. Intell. Neurosci.* **2017**, *2017*, 1–11. [[CrossRef](#)] [[PubMed](#)]
- Lal, A.; Kumar, R.; Mehta, U. Energy dispatch fuzzy model in hybrid power system. *Int. Energy J.* **2014**, *14*, 133–142.
- Ellabban, O.; Abu-Rub, H.; Blaabjerg, F. Renewable energy resources: Current status, future prospects and their enabling technology. *Renew. Sustain. Energy Rev.* **2014**, *39*, 748–764. [[CrossRef](#)]
- Lv, S.; He, W.; Zhang, A.; Li, G.; Luo, B.; Liu, X. Modelling and analysis of a novel compressed air energy storage system for trigeneration based on electrical energy peak load shifting. *Energy Convers. Manag.* **2017**, *135*, 394–401. [[CrossRef](#)]
- Mohan, V.; Singh, J.G.; Ongsakul, W.; Madhu, M.N.; Suresh, M.P.R. Economic and network feasible online power management for renewable energy integrated smart microgrid. *Sustain. Energy Grids Netw.* **2016**, *7*, 13–24. [[CrossRef](#)]
- Luo, X.; Wang, J.; Dooner, M.; Clarke, J.; Krupke, C. Overview of Current Development in Compressed Air Energy Storage Technology. *Energy Procedia* **2014**, *62*, 603–611. [[CrossRef](#)]
- Akinyele, D.; Rayudu, R.; Rayudu, R. Review of energy storage technologies for sustainable power networks. *Sustain. Energy Technol. Assess.* **2014**, *8*, 74–91. [[CrossRef](#)]

11. Hussain, H.; Javaid, N.; Iqbal, S.; Hasan, Q.; Aurangzeb, K.; Alhussein, M. An Efficient Demand Side Management System with a New Optimized Home Energy Management Controller in Smart Grid. *Energies* **2018**, *11*, 190. [[CrossRef](#)]
12. Khamis, A.; Shahrieel, M.; Aras, M.; Nizam, H.; Shah, M.; Zamzuri, M.; Rashid, A. Design and Analysis of Diesel Generator with Battery Storage for Microgrid System. *Int. J. Adv. Eng. Res. Technol.* **2017**, *5*, 26–32.
13. Lim, Y.; Al-Atabi, M.; Williams, R.A. Liquid air as an energy storage: A review. *J. Eng. Sci. Technol.* **2016**, *11*, 496–515.
14. Kassim, A.H.; Miskon, M.T.; Rustam, I.; Mat Zain, M.Y.; Mod Arifin, A.I.; Rizman, Z.I. Optimum storage size for thermal energy storage system. *ARPN J. Eng. Appl. Sci.* **2017**, *12*, 3304–3307.
15. Han, X.; Liao, S.; Ai, X.; Yao, W.; Wen, J. Determining the Minimal Power Capacity of Energy Storage to Accommodate Renewable Generation. *Energies* **2017**, *10*, 468. [[CrossRef](#)]
16. Sun, H.; Luo, X.; Wang, J. Feasibility study of a hybrid wind turbine system—Integration with compressed air energy storage. *Appl. Energy* **2015**, *137*, 617–628. [[CrossRef](#)]
17. Li, S.; Dai, Y. Design and Simulation Analysis of a Small-Scale Compressed Air Energy Storage System Directly Driven by Vertical Axis Wind Turbine for Isolated Areas. *J. Energy Eng.* **2015**, *141*, 04014032. [[CrossRef](#)]
18. Krupke, C.; Wang, J.; Clarke, J.; Luo, X. Modeling and Experimental Study of a Wind Turbine System in Hybrid Connection with Compressed Air Energy Storage. *IEEE Trans. Energy Convers.* **2017**, *32*, 137–145. [[CrossRef](#)]
19. Saadat, M.; Shirazi, F.A.; Li, P.Y. Modeling and control of an open accumulator Compressed Air Energy Storage (CAES) system for wind turbines. *Appl. Energy* **2015**, *137*, 603–616. [[CrossRef](#)]
20. Hadjipaschalis, I.; Poullikkas, A.; Efthimiou, V. Overview of current and future energy storage technologies for electric power applications. *Renew. Sustain. Energy Rev.* **2009**, *13*, 1513–1522. [[CrossRef](#)]
21. Winslow, K.M.; Laux, S.J.; Townsend, T.G. A review on the growing concern and potential management strategies of waste lithium-ion batteries. *Resour. Conserv. Recycl.* **2018**, *129*, 263–277. [[CrossRef](#)]
22. Orlins, S.; Guan, D. China's toxic informal e-waste recycling: Local approaches to a global environmental problem. *J. Clean. Prod.* **2016**, *114*, 71–80. [[CrossRef](#)]
23. Richa, K.; Babbitt, C.W.; Gaustad, G. Eco-Efficiency Analysis of a Lithium-Ion Battery Waste Hierarchy Inspired by Circular Economy. *J. Ind. Ecol.* **2017**, *21*, 715–730. [[CrossRef](#)]
24. Castellani, B.; Morini, E.; Nastasi, B.; Nicolini, A.; Rossi, F. Small-Scale Compressed Air Energy Storage Application for Renewable Energy Integration in a Listed Building. *Energies* **2018**, *11*, 1921. [[CrossRef](#)]
25. Chen, H.; Zhang, X.; Liu, J.; Tan, C. Compressed Air Energy Storage. In *Energy Storage—Technologies and Applications*; Zobaa, A.F., Ed.; InTechOpen: London, UK, 2013; pp. 101–112. ISBN 978-953-51-0951-8.
26. Wang, J.; Lu, K.; Ma, L.; Dooner, M.; Miao, S.; Li, J. Overview of Compressed Air Energy Storage and Technology Development. *Energies* **2017**, *10*, 991. [[CrossRef](#)]
27. Safaei, H.; Aziz, M.J. Thermodynamic Analysis of Three Compressed Air Energy Storage Systems: Conventional, Adiabatic, and Hydrogen-Fueled. *Energies* **2017**, *10*, 1020. [[CrossRef](#)]
28. Salvini, C. CAES Systems Integrated into a Gas-Steam Combined Plant: Design Point Performance Assessment. *Energies* **2018**, *11*, 415. [[CrossRef](#)]
29. Chong, S.-H. High Development of a Numerical Approach to Simulate Compressed Air Energy Storage Subjected to Cyclic Internal Pressure. *Energies* **2017**, *10*, 1620. [[CrossRef](#)]
30. Jerin, R.A.; Thomas, M.; Palanisamy, K.; Umashankar, S. Enhancing Low Voltage Ride Through Capability in Utility Grid Connected Single Phase Solar Photovoltaic System. *J. Eng. Sci. Technol.* **2018**, *13*, 1016–1033.
31. Gafazi, A.; Cheknane, A.; Merzouk, I.; Seddik, B. Control of A Three Levels AC/DC Converter With Virtual-Flux Direct Power Controlling Method for Grid-Connected Wind Power System Under Grid'S Fault. *J. Eng. Sci. Technol.* **2018**, *13*, 2236–2245.
32. Castillo, A.; Gayme, D.F. Grid-scale energy storage applications in renewable energy integration: A survey. *Energy Convers. Manag.* **2014**, *87*, 885–894. [[CrossRef](#)]
33. Phochai, O.; Ongsakul, W.; Mitra, J.; Member, S. Voltage Control Strategies for Grid-Connected Solar PV Systems. In Proceedings of the 2014 International Conference and Utility Exhibition on Green Energy for Sustainable Development, Pattaya, Thailand, 19–21 March 2014; pp. 19–21.

34. Veerasathian, C.; Ongsakul, W.; Mitra, J. Voltage stability assessment of DFIG wind turbine in different control modes. In Proceedings of the 2014 International Conference and Utility Exhibition on Green Energy for Sustainable Development, Pattaya, Thailand, 19–21 March 2014; pp. 1–6.
35. Venkataramani, G.; Parankusam, P.; Ramalingam, V.; Wang, J. A review on compressed air energy storage—A pathway for smart grid and polygeneration. *Renew. Sustain. Energy Rev.* **2016**, *62*, 895–907. [[CrossRef](#)]
36. Martinez, M.; Molina, M.G.; Frack, P.F.; Mercado, P.E.; Molina, M. Dynamic Modeling, Simulation and Control of Hybrid Energy Storage System Based on Compressed Air and Supercapacitors. *IEEE Lat. Am. Trans.* **2013**, *11*, 466–472. [[CrossRef](#)]
37. Martinez, M.; Molina, M.; Mercado, P.E. Dynamic performance of compressed air energy storage (CAES) plant for applications in power systems. In Proceedings of the 2008 IEEE/PES Transmission and Distribution Conference and Exposition: Latin America, Sao Paulo, Brazil, 8–10 November 2010; pp. 496–503.
38. Maia, T.A.; Barros, J.E.; Filho, B.J.C.; Porto, M.P. Experimental performance of a low cost micro-CAES generation system. *Appl. Energy* **2016**, *182*, 358–364. [[CrossRef](#)]
39. Kokaew, V.; Moshrefi-Torbati, M.; Sharkh, S.M. Maximum Efficiency or Power Tracking of Stand-alone Small Scale Compressed Air Energy Storage System. *Energy Procedia* **2013**, *42*, 387–396. [[CrossRef](#)]
40. Kokaew, V.; Sharkh, S.; Moshrefi-Torbati, M. A hybrid method for maximum power tracking of a small scale CAES system. In Proceedings of the 2014 9th International Symposium on Communication Systems, Networks & Digital Sign (CSNDSP), Manchester, UK, 23–25 July 2014; pp. 61–66.
41. Kokaew, V.; Sharkh, S.M.; Moshrefi-Torbati, M. Maximum Power Point Tracking of a Small-Scale Compressed Air Energy Storage System. *IEEE Trans. Ind. Electron.* **2016**, *63*, 985–994. [[CrossRef](#)]
42. Vongmanee, V.; Monyakul, V. A New Concept of Small-Compressed Air Energy Storage System Integrated with Induction Generator. In Proceedings of the 2008 IEEE International Conference on Sustainable Energy Technologies, Singapore, 24–27 November 2008; pp. 866–871.
43. Lemofouet, S.; Rufer, A. A Hybrid Energy Storage System Based on Compressed Air and Supercapacitors with Maximum Efficiency Point Tracking (MEPT). *IEEE Trans. Ind. Electron.* **2006**, *53*, 1105–1115. [[CrossRef](#)]
44. Moradi, M.H.; Eskandari, M.; Hosseinian, S.M. Cooperative control strategy of energy storage systems and micro sources for stabilizing microgrids in different operation modes. *Int. J. Electr. Power Energy Syst.* **2016**, *78*, 390–400. [[CrossRef](#)]
45. Tayab, U.B.; Al Humayun, M.A. Operation and control of cascaded H-bridge multilevel inverter with proposed switching angle arrangement techniques. *J. Eng. Sci. Technol.* **2017**, *12*, 3148–3157.
46. Siri, K. Voltage-mode grid-tie inverter with active power factor correction. In Proceedings of the 2015 IEEE 24th International Symposium on Industrial Electronics (ISIE), Buzios, Brazil, 3–5 June 2015; pp. 1133–1139.
47. Kilic, E.; Yilmaz, S.; Ozcalik, H.R.; Sit, S. A comparative analysis of FLC and ANFIS controller for vector controlled induction motor drive. In Proceedings of the 2015 Intl Aegean Conference on Electrical Machines & Power Electronics (ACEMP), 2015 Intl Conference on Optimization of Electrical & Electronic Equipment (OPTIM) & 2015 Intl Symposium on Advanced Electromechanical Motion Systems (ELECTROMOTION), Side, Turkey, 2–4 September 2015; pp. 102–106.
48. Grosenick, L.; Marshel, J.H.; Deisseroth, K. Closed-Loop and Activity-Guided Optogenetic Control. *Neuron* **2015**, *86*, 106–139. [[CrossRef](#)] [[PubMed](#)]
49. Liu, C.; Wang, J.; Deng, B.; Wei, X.-L.; Yu, H.-T.; Li, H.-Y. Variable universe fuzzy closed-loop control of tremor predominant Parkinsonian state based on parameter estimation. *Neurocomputing* **2015**, *151*, 1507–1518. [[CrossRef](#)]
50. Khamis, A.; Badarudin, Z.M.; Ahmad, A.; Ab Rahman, A.; Bakar, N. Development of mini scale compressed air energy storage system. In Proceedings of the 2011 IEEE Conference on Clean Energy and Technology (CET), Kuala Lumpur, Malaysia, 27–29 June 2011; pp. 151–156.
51. Namazov, M. DC motor position control using fuzzy proportional-derivative controllers with different defuzzification methods. *Turk. J. Fuzzy Syst.* **2010**, *1*, 36–54.
52. Agarwal, P.A.P. Brushless Dc Motor Speed Control Using Proportional-Integral and Fuzzy Controller. *IOSR/JEEE* **2013**, *5*, 68–78. [[CrossRef](#)]
53. Kamble, L.V.; Pangavhane, D.R. Heat transfer studies using artificial neural network—A review. *Int. Energy J.* **2014**, *14*, 25–42.

54. Jafarian, M.; Ranjbar, A. Fuzzy modeling techniques and artificial neural networks to estimate annual energy output of a wind turbine. *Renew. Energy* **2010**, *35*, 2008–2014. [[CrossRef](#)]
55. Tino, P.; Benuskova, L.; Sperduti, A. *Artificial Neural Network Models*; Springer Handbooks: Berlin, Germany, 2015; Volume 8, pp. 455–472.
56. Yang, H.; Fu, Y.-T.; Zhang, K.-P.; Li, Z.-Q. Speed tracking control using an ANFIS model for high-speed electric multiple unit. *Control Eng. Pract.* **2014**, *23*, 57–65. [[CrossRef](#)]
57. Kassem, Y.; Çamur, H.; Bennur, K.E. Adaptive Neuro-Fuzzy interference System (ANFIS) and Artificial Neural Network (ANN) for predicting the kinematic viscosity and density of biodiesel-petroleum diesel blends. *Am. J. Comput. Sci. Technol.* **2018**, *1*, 8–18.



© 2019 by the authors. Licensee MDPI, Basel, Switzerland. This article is an open access article distributed under the terms and conditions of the Creative Commons Attribution (CC BY) license (<http://creativecommons.org/licenses/by/4.0/>).

